Testing Higher-Order Lagrangian Perturbation Theory Against Numerical Simulations - 1. Pancake Models

T. Buchert[1], A.L. Melott[2], A.G. Wei[1]
[1]Max-Planck-Institut für Astrophysik
Karl-Schwarzschild-Str. 1
85740 Garching, Munich, F. R. G.
[2]Department of Physics and Astronomy
University of Kansas
Lawrence, Kansas 66045 U. S. A.

TESTING HIGHER-ORDER LAGRANGIAN PERTURBATION THEORY AGAINST NUMERICAL SIMULATIONS - 1. PANCAKE MODELS

by

T. Buchert[1], A.L. Melott[2], A.G. Weiß[1]

[1]Max-Planck-Institut für Astrophysik
Karl-Schwarzschild-Str. 1
85740 Garching, Munich
F. R. G.

[2]Department of Physics and Astronomy
University of Kansas
Lawrence, Kansas 66045
U. S. A.

submitted to *Astron. Astrophys., Main Journal*

Testing higher-order Lagrangian perturbation theory against numerical simulations - 1. Pancake models

by

T. Buchert, A.L. Melott, A.G. Weiß

Summary: We present results showing an improvement of the accuracy of perturbation theory as applied to cosmological structure formation for a useful range of quasi-linear scales. The Lagrangian theory of gravitational instability of an Einstein-de Sitter dust cosmogony investigated and solved up to the third order in the series of papers by Buchert (1989, 1992, 1993a), Buchert & Ehlers (1993), Buchert (1993b), Ehlers & Buchert (1993), is compared with numerical simulations. In this paper we study the dynamics of pancake models as a first step. In previous work (Coles *et al.* 1993, Melott *et al.* 1993, Melott 1993) the accuracy of several analytical approximations for the modeling of large-scale structure in the mildly non-linear regime was analyzed in the same way, allowing for direct comparison of the accuracy of various approximations. In particular, the "Zel'dovich approximation" (Zel'dovich 1970, 1973, hereafter ZA) as a subclass of the first-order Lagrangian perturbation solutions was found to provide an excellent approximation to the density field in the mildly non-linear regime (i.e. up to a linear r.m.s. density contrast of $\sigma \approx 2$). The performance of ZA in hierarchical clustering models can be greatly improved by truncating the initial power spectrum (smoothing the initial data). We here explore whether this approximation can be further improved with higher-order corrections in the displacement mapping from homogeneity. We study a single pancake model (truncated power-spectrum with power-index $n = -1$) using cross-correlation statistics employed in previous work.

We found that for all statistical methods used the higher-order corrections improve the results obtained for the first-order solution up to the stage when σ(linear theory) ≈ 1. While this improvement can be seen for all spatial scales, later stages retain this feature only above a certain scale which is increasing with time. However, third-order is not much improvement over second-order at any stage. The total breakdown of the perturbation approach is observed at the stage, where σ(linear theory)≈ 2, which corresponds to the onset of hierarchical clustering. This success is found at a considerably higher non-linearity than is usual for perturbation theory. Whether a truncation of the initial power-spectrum in hierarchical models retains this improvement will be analyzed in a forthcoming work.

1. Introduction

In most recent research in cosmology, the gravitational instability picture of the standard Friedman-Lemaître cosmogonies has been used to describe the earliest stages of the formation of inhomogeneities in the Universe (see, e.g, Peebles 1980 and ref. therein). The first quantitative exploration used linear perturbation theory to make predictions from theory. Although there are serious restrictions of applicability of this perturbation approach (e.g., the density contrast $\delta = \frac{\rho - \rho_H}{\rho_H}$, where ρ_H is the homogeneous density of the background cosmogony, should be much less than 1), the solutions are still applied to normalize inhomogeneous cosmological models, i.e., to determine the amplitude of the initial fluctuation field in comparison with the density contrast we observe today. We now know that first-order solutions of this perturbation approach cannot be used as an approximation of the present day density field. Only, if we smooth the field with an extremely large smoothing length of the order of 100 h^{-1}Mpc (Coles *et al.* 1993), a comparison with non-linearly evolved density fields can be meaningful. This perturbation approach is Eulerian, i.e., the perturbations are evaluated as functions of Eulerian coordinates.

In the 70's Zel'dovich realized the limitations of this approach and proposed an extrapolation of the Eulerian linear solutions into the mildly non-linear regime by employing the Lagrangian picture of continuum mechanics (Zel'dovich 1970, 1973). In his model the motion of the continuum is similar to the purely kinematical motion of a system of particles which move under inertia. The model can be mapped to this system by a suitable transformation of dependent and independent variables (Shandarin & Zel'dovich 1984, 1989). The success of Zel'dovich's extrapolation for the description of typical patterns of the large-scale structure has been widely recognized, although not generally understood. It can be traced back to the fact that the Lagrangian description is based on following the trajectories of fluid elements, while the density itself does not appear as a dynamical variable in this picture and can be integrated exactly along the trajectories of a given solution. Consequently, the density is not limited in a Lagrangian perturbation approach, only the gradient of the displacement field has to be small compared with the expansion factor of the homogeneous background (Buchert 1992, Ehlers & Buchert 1993). Moreover, Zel'dovich's model can be systematically derived by solving the Lagrangian evolution equations to the first-order (Buchert 1992). It also provides a class of exact three-dimensional solutions in the case where the collapse is maximally anisotropic (i.e., in the case where locally two of three eigenvalues of the fluid's deformation tensor vanish) (Buchert 1989). The plane-symmetric case is contained in a subclass of these solutions; first-order Lagrangian perturbation solutions are the general solutions of the full system in this case.

Lagrangian perturbation solutions are now available for various backgrounds and up to the third order in the deviations from homogeneity (see Buchert 1993b and references therein). Parallel efforts to investigate Lagrangian perturbation solutions are made by Moutarde *et al.* (1991), Bouchet *et al.* (1992), Lachièze-Rey (1993), Gramann (1993), Giavalisco *et al.* (1993), Croudace *et al.* (1993), see also Bertschinger & Jain (1993).

Coles, Melott and Shandarin (1993) conducted a series of tests of analytical approximations by cross-correlating them with N-body simulations. They tested the Eulerian linear perturbation solution and the "Zel'dovich approximation" (hereafter ZA) as a subclass of the irrotational Lagrangian linear solution. They found that the latter was considerably more successful than the former. Considerable further improvement is made if the ZA is applied not to the full power spectrum on the whole range of spatial scales, but only to a truncated body of the spectrum. The truncation removes unwanted non-linearities, which are evolved beyond the range of applicability of the model (Melott and Shandarin 1990, Beacom *et al.* 1991, Kofman *et al.* 1992, Coles *et al.* 1993). The shape of high-frequency

filters imposed on the power-spectrum was found to be important (Melott *et al.* 1993). Most successful in respect of improvement of the cross-correlation statistics was the use of Gaussian filters, but if one wishes to work backwards from evolved to initial state, a sharp truncation (step function) in k is preferable (Melott 1983).

Since closer study of analytical approximations reveals both limitations and powerful properties, it is worthwhile to study generalizations of Zel'dovich's mapping to improve the cross-correlation with numerical simulations. In this way the modeling of large-scale structure is effective and can be used to provide initial and boundary conditions for the evolution of small-scale structure within the large-scale environment, which could be modelled, e.g., by fully hydrodynamical simulations. Although the applicability of the analytical models under study is not limited to a particular type of spectrum (the "Zel'dovich approximation" was originally used for modeling the standard "pancake picture", see Shandarin & Zel'dovich 1989), we here do concentrate our comparison on "pancake models", i.e., models which do not involve small-scale power in the initial data. We do this as a first step to properly understand the limitations of higher-order corrections to Zel'dovich's mapping. Also, pancake models can be understood as generic archetype of hierarchical models which involve pancaking on all spatial scales (Kofman *et al.* 1992). Because the models we study here already have a truncated initial power spectrum, we do not apply additional truncation as in Coles *et al.* (1993) or Melott, Pellman and Shandarin (1993). In a second step, we shall later analyze various power spectra which are evolved deeply into the non-linear regime in order to probe the performance of the Lagrangian approximations in the case of hierarchical models (paper II *in preparation*).

Further work on other approximations is also in preparation: the frozen–flow approximation (Matarrese *et al.* 1992) and the adhesion approximation (Kofman *et al.* 1992 and references therein) will be given a similar treatment.

Another advantage of analytical models is the possibility of high-spatial resolution of the density field. Analytical mappings of a continuum offer in principle infinite resolution in contrast to numerical N-body simulations. We shall explain that models with sufficiently smooth initial data like pancake models can be resolved easily to, e.g., an effective resolution of 2048^3 particles. However, as we shall see later, the accuracy of this effort would be limited to early stages of non-linearity.

2. Numerical realization of pancake models

We specify initial data in terms of a power spectrum $\mathcal{P}(k)$ (as a function of comoving wavenumber $k = |\vec{k}|$) of Gaussian density perturbations of the form:

$$\mathcal{P}(k) = < |\delta_{\vec{k}}|^2 > \propto |\vec{k}|^n \quad , \tag{1}$$

where $\delta_{\vec{k}}$ is the discrete spatial Fourier transform of the density contrast δ. We shall take $n = -1$, and truncate the power spectrum at a characteristic frequency k_c. In this way we will probe the epoch of first pancaking. We also define the non-linearity scale $k_{nl}(t)$:

$$a^2(t) \int_0^{k_{nl}(t)} d^3k \, \mathcal{P}(k) \; = \; 1 \quad , \tag{2}$$

where $k_{nl}(t)$ is decreasing with time as successively larger scales enter the non-linear regime; $a(t)$ is the scale factor of the homogeneous background: for the initial data we set $k_c = 4k_f$, and $a(t_i) := 1$ where k_f is the fundamental mode of the simulation box. We emphasize that we give initial data early (at the r.m.s. density contrast of $\sigma_i(k_c) = 0.01$) to guarantee an objective modeling of the collapse of first pancakes in the model. One of us (Melott 1985, 1987) has emphasized the importance of beginning numerical simulations at a highly linear stage to avoid an artificial delay of the collapse time of first objects. This delay is inherent in Zel'dovich's displacement mapping which is used to initialize the numerical simulation (compare Blanchard *et al.* (1993) for a discussion of this problem). From several first studies of higher-order perturbation solutions we know that the collapse is significantly accelerated by the higher-order corrections even in a generic field (Buchert *et al.* 1993). An objective test of this feature can only be conducted by giving the initial data early. The results of making too late a start with too high an amplitude are not detectable in the two–point correlation function since this is mostly determined by long waves just going non-linear (Beacom *et al.* 1991; Melott & Shandarin 1993).

The evolution of inhomogeneities is modelled in a flat Einstein-de Sitter background ($a(t) = (\frac{t}{t_i})^{2/3}$). We evolve the field with an enhanced PM (particle-mesh) method (Melott 1986) using 128^3 particles each on a comoving 128^3 mesh with periodic boundary conditions. This method makes the code resolution-equivalent to a traditional PM code with 128^3 particles on a 256^3 mesh (see Weinberg *et al.* (1993)).

In what follows we will specify the stages we study by the *Eulerian linear theory* amplitude which is just proportional to the scale factor in these $\Omega = 1$ models. (The r.m.s. density contrast σ_2 denotes σ(linear theory) in the numerical simulation throughout this paper.) Of course, the real density contrast is larger due to mode coupling effects.

From this simulation we extract six stages, the first at the epoch when pancake formation is just beginning ($\sigma_2 = 0.25$), the second at the moment when the first pancakes have collapsed ($\sigma_2 = 0.5$), the third at a stage when the cellular connection of different pancakes is established (corresponding to the contemporary epoch according to the standard normalization) ($\sigma_2 = 1$), the fourth and fifth at more advanced stages, where secondary shell-crossings have developed ($\sigma_2 = 1.2$ and $\sigma_2 = 1.5$), and the last at a stage when the non-linearity scale has dropped to $k_{nl} = 2k_f$ ($\sigma_2 = 2$). This stage corresponds to the onset of hierarchical clustering due to merging of pancakes.

3. The Lagrangian perturbation solutions

In what follows we make use of a restriction of the initial data commonly used in realizations of large-scale structure models as well as in the numerical realization quoted above. We require that, initially, the peculiar-velocity $\vec{u}(\vec{X}, t_i)$ be proportional to the peculiar-acceleration $\vec{w}(\vec{X}, t_i)$:

$$\vec{u}(\vec{X}, t_i) = \vec{w}(\vec{X}, t_i) t_i \quad , \tag{3}$$

where we have defined the fields as usual (compare Peebles 1980, Buchert 1992). This restriction has proved to be appropriate for the purpose of modeling large-scale structure since, for irrotational flows, the peculiar-velocity field tends to be parallel to the gravitational peculiar-acceleration after some time. The reason for this tendency is related to the existence of growing and decaying perturbations in the linear regime, the growing part

supports the tendency to parallelity. The assumption of irrotationality should be adequate down to the non-linearity scale.

Henceforth, a comma denotes derivative with respect to Lagrangian coordinates, and $\Delta_0 := \nabla_0^2$, where ∇_0 denotes the nabla operator with respect to Lagrangian coordinates. We shall use in the following the initial peculiar-velocity potential $\mathcal{S}$ defined as $\vec{u}(\vec{X}, t_i) =: \nabla_0 \mathcal{S}(\vec{X})$. The initial peculiar-gravitational potential ϕ, $\vec{w}(\vec{X}, t_i) =: -\nabla_0 \phi(\vec{X})$ is related to it as $\mathcal{S} = -\phi t_i$ (eq. (3)). Further, we introduce the symbols $I(\mathcal{S}_{,i,k}) = tr(\mathcal{S}_{,i,k}) = \Delta_0 \mathcal{S}$, $II(\mathcal{S}_{,i,k}) = \frac{1}{2}[(tr(\mathcal{S}_{,i,k}))^2 - tr((\mathcal{S}_{,i,k})^2)]$ and $III(\mathcal{S}_{,i,k}) = \det(\mathcal{S}_{,i,k})$ which denote the three principal scalar invariants of the tensor $(\mathcal{S}_{,i,k})$.
We introduce the field of trajectories $\vec{x} = \vec{f}(\vec{X}, t)$, where $\vec{x}$ denote Eulerian and $\vec{X}$ Lagrangian coordinates. We express the solutions in a comoving reference system $\vec{q} = \vec{F}(\vec{X}, t)$, where $\vec{q} = \vec{x}/a(t)$ denote comoving Eulerian coordinates.

With a superposition ansatz for Lagrangian perturbations of an Einstein-de Sitter background the following family of trajectories $\vec{q} = \vec{F}(\vec{X}, a)$ as irrotational solution of the Euler-Poisson system up to the third order in the perturbations from homogeneity has been given by one of us (Buchert 1993b). The general set of initial data $(\phi(\vec{X}), \mathcal{S}(\vec{X}))$ is only restricted according to $\mathcal{S} = -\phi t_i$ (eq. (3)):

$$\vec{F} = \vec{X} \; + \; q_1(a) \, \nabla_0 \mathcal{S}^{(1)}(\vec{X}) \; + \; q_2(a) \, \nabla_0 \mathcal{S}^{(2)}(\vec{X})$$

$$+ \, q_3^a(a) \, \nabla_0 \mathcal{S}^{(3a)}(\vec{X}) \; + \; q_3^b(a) \, \nabla_0 \mathcal{S}^{(3b)}(\vec{X}) \; - \; q_3^c(a) \, \nabla_0 \times \vec{\mathcal{S}}^{(3c)}(\vec{X}) \; , \qquad (4)$$

with the time-dependent coefficients expressed in terms of the expansion function $a(t) = (\frac{t}{t_i})^{2/3}$:

$$q_1 = \left(\frac{3}{2}\right)(a-1) \quad , \qquad (4a)$$

$$q_2 = \left(\frac{3}{2}\right)^2 (-\frac{3}{14}a^2 + \frac{3}{5}a - \frac{1}{2} + \frac{4}{35}a^{-\frac{5}{2}}) \quad , \qquad (4b)$$

$$q_3^a = \left(\frac{3}{2}\right)^3 (-\frac{1}{9}a^3 + \frac{3}{7}a^2 - \frac{3}{5}a + \frac{1}{3} - \frac{16}{315}a^{-\frac{5}{2}}) \quad , \qquad (4c)$$

$$q_3^b = \left(\frac{3}{2}\right)^3 (\frac{5}{42}a^3 - \frac{33}{70}a^2 + \frac{7}{10}a - \frac{1}{2} + \frac{4}{35}a^{-\frac{1}{2}} + \frac{4}{105}a^{-\frac{5}{2}}) \quad , \qquad (4d)$$

$$q_3^c = \left(\frac{3}{2}\right)^3 (\frac{1}{14}a^3 - \frac{3}{14}a^2 + \frac{1}{10}a + \frac{1}{2} - \frac{4}{7}a^{-\frac{1}{2}} + \frac{4}{35}a^{-\frac{5}{2}}) \quad . \qquad (4e)$$

The perturbation potentials have to be constructed by solving iteratively the following set of 7 Poisson equations:

$$\Delta_0 \mathcal{S}^{(1)} = I(\mathcal{S}_{,i,k}) \, t_i \quad , \qquad (4f)$$

$$\Delta_0 \mathcal{S}^{(2)} = 2II(\mathcal{S}^{(1)}_{,i,k}) \quad , \qquad (4g)$$

$$\Delta_0 \mathcal{S}^{(3a)} = 3III(\mathcal{S}^{(1)}_{,i,k}) \quad , \qquad (4h)$$

$$\Delta_0 \mathcal{S}^{(3b)} = \sum_{a,b,c} \epsilon_{abc} \frac{\partial(\mathcal{S}^{(2)}_{,a}, \mathcal{S}^{(1)}_{,b}, X_c)}{\partial(X_1, X_2, X_3)} \quad , \tag{4i}$$

$$(\Delta_0 \vec{\mathcal{S}}^{(3c)})_k = \epsilon_{pq[j} \frac{\partial(\mathcal{S}^{(2)}_{,i]}, \mathcal{S}^{(1)}_{,p}, X_q)}{\partial(X_1, X_2, X_3)} \quad . \tag{4j,k,l}$$

($i, j, k = 1, 2, 3$ with cyclic ordering).

We realize the solution by first solving Poisson's equation for $\mathcal{S}$ via FFT (Fast Fourier Transform) from the initial density contrast δ generated as initial data for the numerical simulation (Section **2**). In a flat background model we have:

$$\Delta_0 \mathcal{S} = -\frac{2}{3t_i}\delta \quad . \tag{5}$$

We first note that the first-order part of the mapping (4) is equivalent to Zel'dovich's approximation, if we put $\mathcal{S}^{(1)} = \mathcal{S}t_i$. The only formal difference is that we start at the initial time on an undeformed grid due to the assumption $a(t_i) = 1$: $\vec{F}(\vec{X}, t_i) = \vec{X}$. This solution of the first Poisson equation (4f) as well as the entire solution (4) is unique provided we impose periodic boundary conditions on $\mathcal{S}$ and fix some gauge conditions accordingly (Ehlers & Buchert 1993). With this setting the source expressions in (4f-h) are computable in terms of the initial data $\mathcal{S}$. We solve all derivatives and all Poisson equations in $k-$space by using FFT, the four Poisson equations (4i-l) have to be solved iteratively by using the second-order perturbation potential calculated first from (4g).

The first-order part of the solution (4) covers the kinematical aspect of the collapse process, whereas the second-order part covers essential aspects of the tidal action of the gravitational field (Buchert & Ehlers 1993). At the third order, there are also interaction terms among the perturbation potentials at first and second order, which induce vorticity in Lagrangian space. Although the solution (4) is rotational in Lagrangian space, the Eulerian fields remain irrotational until the first shell-crossings. The development of caustics will result in multi-stream flow and will introduce vorticity also in Eulerian space (see, e.g., Chernin 1993). Note that the Eulerian representation of the equations breaks down at caustics, while the Lagrangian representation of the fluid's motion in terms of trajectories is still regular and formally allows to follow the motion of the fluid across caustics which we shall do. However, we emphasize that the Lagrangian solution $\vec{f}$ represents solutions of the Euler-Poisson system only as long as the mapping to Eulerian space is single-valued; In multi-stream regions a formal extrapolation of $\vec{f}$ across caustics neglects the gravitational interaction of the streams since, in these regions, the gravitational field-strength acting on *each* particle is the sum of the field-strengths of the streams (compare Ehlers & Buchert 1993).

In order to understand that the higher-order approximation schemes are better than the first-order scheme until shell-crossing (regardless of the initial conditions and the scale of the fluctuations), the following general equation can be used: Consider the density contrast $\Delta := (\varrho - \varrho_H)/\varrho$, $-\infty < \Delta < 1$, which is more adapted to the non-linear situation than the conventional definition $\delta = (\varrho - \varrho_H)/\varrho_H = \Delta/(1-\Delta)$, defined in Eulerian perturbation theory. For this the following fully non-linear evolution equation derived from the continuity equation and Poisson's equation has been found (Buchert 1992; see

also Peebles 1987, Buchert 1989, Bertschinger & Jain 1993):

$$\dot{\Delta} = (\Delta - 1)\mathbf{I} \ , \tag{6a}$$

$$\ddot{\Delta} + 2\frac{\dot{a}}{a}\dot{\Delta} - 4\pi G\varrho_H \Delta = (\Delta - 1)2\mathbf{II} \ , \tag{6b}$$

where here **I** and **II** denote the first and second principal scalar invariants, respectively, of the peculiar-velocity tensor gradient $(u_{i,j})$ (contrary to the notation before, a comma here denotes derivative with respect to comoving Eulerian coordinates $\vec{q}$, a dot denotes Lagrangian time-derivative $\frac{d}{dt} := \frac{\partial}{\partial t}|_q + \frac{\vec{u}}{a} \cdot \nabla_q$):

$$\mathbf{I} := \frac{1}{a}\sum_i u_{i,i} \quad , \quad \mathbf{II} := \frac{1}{2a^2}\left((\sum_i u_{i,i})^2 - \sum_{ij}(u_{i,j}u_{j,i}) \right) \ . \tag{6c}$$

This equation is exact. For the approximation schemes we can read off the following: The first-order model solves equation (6) with $\mathbf{II} \to 0$, whereas the second-order model takes the second invariant into account for small displacements from the first-order trajectories. Thus, the second-order theory improves upon first-order until equation (6) breaks down at shell-crossing.

We realize the solution (4) at each order by calculating 128^3 trajectories. Note that, although we have 7 Poisson equations to solve, the model (4) is very time-efficient: On a CONVEX C3 the third-order model takes about 20 minutes to realize the density distribution for each stage at this resolution, while the first-order model takes 2 and the second-order model 3 minutes. On a CRAY YMP/464 the corresponding CPU times are smaller by a factor of 5. The N-body simulation run here takes 138 integration steps each of which uses about 2 minutes on a CRAY 2, i.e. in total 5.4 hours to get to the final stage. The N-body code is limited by the speed of the (rather poor) FFT on a CRAY 2. Since this was written, we have moved our N-body computing to a CONVEX C3.

A higher resolution can be easily obtained for the analytical model, provided the smallest wavelength in the model (corresponding to $k_c = 4k_f$ here) is calculated to sufficient accuracy. For example, if we resolve the box with length L with 128 calculated density values along one spatial direction, the smallest wavelength $L/4$ will be calculated at 32 points; 32 points will be sufficient to map the coherence scale at high accuracy. Interpolating the calculated grid points, e.g., 16 times, we obtain an effective resolution in the box of 2048^3 particles. This interpolation method gives highly accurate results for the final distribution, since the analytical mapping contains all non-linear information; it maps the interpolated grid points as if it were calculated ones. For a detailed discussion and illustration of this method see (Buchert & Bartelmann 1991).

Figures 1a to 1d show a comparison of slices of the N-body model and the first- through third-order approximate schemes by visual appearance. Often very high-order information which is difficult to quantify can be rapidly gained from visual presentations.

4. Cross-correlation statistics

4.1. Cross-correlation coefficient

As in Coles *et al.* (1993) and Melott *et al.* (1993) we use here the usual cross-correlation coefficient S to compare the resulting density fields:

$$S := \frac{<(\delta_1 \delta_2)>}{\sigma_1 \sigma_2} \quad , \tag{7}$$

where $\delta_\ell, \ell = 1,2$ represent the density contrasts in the analytical and the numerical approximations, respectively, $\sigma_\ell = \sqrt{<\delta_\ell^2> - <\delta_\ell>^2}$ is the standard deviation in a Gaussian random field; averages $< ... >$ are taken over the entire distribution.

The density in the analytical models is calculated by collecting trajectories of the Lagrangian perturbation solutions at the different orders into a 128^3 pixel grid with the same mesh method (CIC binning) as in the N-body simulation.

The correlation coefficient obeys the bound $|S| \leq 1$; $S = 1$ implies that $\delta_1 = C\delta_2$, with C constant; C close to 1 implies, of course, better agreement between the approximation and the numerical simulation.

Following Coles *et al.* (1993) we will compare the approximation with the simulation with varying amounts of Gaussian smoothing of each so that we can follow accuracy at various lengthscales, and allow for the possibility of results which are essentially correct but for small displacements. We will plot S as a function of σ_2, the r.m.s. density contrast in the numerical simulation. The cross-correlation coefficient S is calculated down to the resolution scale of a 128^3 pixellization of the density field.

There will be basic differences from the procedure of Coles *et al.* . No truncation of the spectrum will be considered here because in pancake models the initial conditions are already truncated. We will not be able to compare these results with those since we are dealing with a different class of models. Instead, we will compare the accuracy of first–, second–, and third–order Lagrangian approximations with the simulation, and thereby gain information on the benefits of going to higher–order Lagrangian solutions within the context of pancake models. In paper II on hierarchical models we will determine to what extent these results carry over to hierarchical models, and we will find out whether substantial improvements over the optimally truncated first-order approach (Melott *et al.* 1993) is made.

In order to couple our cross–correlations to the physical scale, we show the actual r.m.s. density fluctuations for all approximations σ_ℓ as a function of the Gaussian smoothing scale in grid units in Figure 2 for each of our stages. The Gaussian smoothing is done by convolution with $e^{-R^2/2R_G^2}$. The stages correspond to (Eulerian) linear theory $\sigma_2 = 0.25, 0.5, 1.0, 1.2, 1.5$, and 2.0 as discussed before. R_G is given in grid units; remember that the box is 128 grid units in size, and the smallest wavelength perturbation in the initial data was 32 grid units. Since it is known that these Lagrangian schemes give rather accurate locations for pancakes, we are more interested in studying details of structure. Therefore most of our information will be relevant for $R_G < 32$ grid units.

In Figures 3a to 3f we show our most important basic result, the cross-correlation coefficient of the various orders of approximation with the N-body simulation at various stages.

4.2. Power spectrum analysis

Since Lagrangian perturbation solutions include substantial non-linearities (see, e.g., Buchert 1992), we expect that they do not preserve the initial power spectrum of the fluctuation field as the Eulerian linear solution would do. Therefore, it has meaning to test the agreement with the N-body simulation. For the spectrum considered in the present paper ($n = -1$) Melott *et al.* (1993) found that the power spectrum of the truncated ZA with that of the N-body simulation is substantially underestimated. In this respect the spectrum with index $n = -1$ provides an extreme case. We, here, analyze whether the higher-order corrections can improve on that, and present the results of the power spectrum analysis in Figures 4a to 4f.

4.3. Relative phase-errors

The non-linear evolution of the fluctuation field does not preserve the initial power spectrum as well as the phase information, which is not contained in the power spectrum. There will be a substantial change in the phases due to non-linear phase-locking effects, which are already described by the first-order Lagrangian perturbation solutions (see Melott *et al.* 1993). Also here we expect an improvement due to higher-order corrections, since they contain essential effects of tidal interactions which should contribute to the change of the phases.

We calculate the *relative phase error* as follows: The Fourier coefficients of the initial fluctuation field $\delta_{\vec{k}} = |\delta_{\vec{k}}|e^{i\phi_{\vec{k}}}$ contain information about the amplitude $|\delta_{\vec{k}}|$ and the phase angle $\phi_{\vec{k}}$. We measure the angle $\theta = \phi_1 - \phi_2$, where ϕ_2 are the phases in the N-body simulation, and ϕ_1 in the analytical approximations. We present the results on the relative phase errors in terms of $\cos(\theta)$ as a function of k (calculated in spherical shells in $k-$space). The opposite assignment $\theta = \phi_2 - \phi_1$ yields equivalent results since $\cos(\theta)$ is symmetric around $\theta = 0$. Perfect agreement between the N-body result and the analytical scheme implies $\cos(\theta) = 1$, anti-correlated phases have $\cos(\theta) = -1$, and for randomized phases $\cos(\theta)$ would average to 0. We present the result in Figures 5a to 5f.

4.4. Density distribution functions

The cross-correlation coefficient (**4.1**) measures differences in position up to a constant ratio C of the compared densities (compare Section **2**). In order to probe the differences of the various approximations with respect to the actually predicted densities on different spatial scales, we calculate the density distribution function for each approximation and depict them in Figures 6a to 6d in terms of the number of cells N found with mass density ρ (in units of the mean) as a function of scale.

5. Discussion of the results

In Figures 1a to 1d we show slices of the density fields corresponding to the stages $2, 3, 4$ and 5, while the statistical analysis is done for all six stages.

At the first stage ($\sigma_2 = 0.25$) pancake formation is just beginning. Here, the higher-order schemes predict structures which are almost identical to the N-body result, whereas

the first-order scheme appears to delay the collapse time as was expected. The cross-correlation coefficient as well as the power spectrum measures this feature clearly (Figs. 3a, 4a); the phase information is represented better at higher orders especially on small scales (Fig. 5a). Also the density distribution functions confirm this behavior (Fig. 6a). The number of high-density cells is underestimated by all schemes.

Stage 2 ($\sigma_2 = 0.5$, Figs. 1a) emphasizes this: Here, the higher-order schemes significantly improve on the first-order "Zel'dovich approximation"; the cross-correlation coefficient (Fig. 3b) is as high as $S = 0.90$ for the second-order and only slightly higher for the third-order scheme, while the first-order coefficient has $S = 0.85$ on the scale where $\sigma_2 = 1$. A similar conclusion can be drawn from the power spectrum analysis (Fig. 4b). However, the power on small scales is already underestimated by all schemes, but represented better at higher orders. Interestingly, the phase information contained in the first-order approximation shows randomized relative phase-errors, while the higher-order schemes show a strong tendency to anti-correlated phases at this stage (Fig. 5b). This point would become clearer by analyzing the velocity fields. The better agreement with respect to the cross-correlation and the power spectrum is also a consequence of a better prediction of the collapse time in the higher-order solutions. The density distribution functions (Fig. 6b) show good agreement with the N-body distribution for the second- and third-order models. The first-order model still suffers from its properties mentioned before at stage 1.

At stage 3 (corresponding to the present stage according to the standard normalization, $\sigma_2 = 1$) we can already see slight differences in the density fields (Figs. 1b): The biggest difference is apparent in the lower-right corner where the most evolved structure contained in this slice is seen. We appreciate that in the higher-order solutions filaments stay more compact like in the N-body slice in contrast to the first-order solution. The cross-correlation coefficient (Fig. 3c) shows an almost constant improvement of the second-order upon the first-order approximation down to the smallest scales, while the third-order scheme becomes worse than the second-order result on scales $\sigma_2 > 2$, but still is better than that of first-order up to $\sigma_2 \approx 4$. The power spectrum (Fig. 4c) remains better represented in the higher-order solutions. Starting from this stage, the relative phase-errors show a tendency to randomization for all orders of the perturbation solutions, while the scale where randomization occurs increases with time (Figs. 5c-f). The density distribution functions (Fig. 6c) show excellent agreement with the numerical result but begin to overestimate the number of cells with moderately high density, a feature which is due to the overestimated size of the pancakes.

Stage 4 ($\sigma_2 = 1.2$) is the most interesting stage, where all orders of approximation schemes provide equally good results. The agreement of the density fields with the N-body simulation is still reasonable in all schemes. The most evolved structure shows compact internal density peaks inside the first-order pancakes (Figs. 1c). The cross-correlation coefficients (Fig. 3d) are still high, but only slightly higher in the second- and third-order approximations on large scales corresponding to $\sigma_2 < 3$ (second-order), $\sigma_2 < 2.5$ (third-order). On smaller scales the second-order coefficient stays close to the first-order coefficient, while the third-order scheme starts to fall off more rapidly below the cross-correlation of the first-order scheme. The power spectra (Fig. 4d) are almost identical for all schemes, a property which roughly remains in the following stages. Here, the density distribution functions (Fig. 6d) mirror an amplification of the effect mentioned for stage 3.

The next stage 5 ($\sigma_2 = 1.5$) we can identify with the stage where the break-down of the Lagrangian perturbation solutions has started. Figs. 1d show differences in the thickness of pancakes, which begin to grow more rapidly in the perturbation solutions than in the N-body simulation. The density distribution functions (Fig. 6e) overestimate the number of low-density cells, while the number of high-density cells is underestimated. The scale above which an improvement of the higher-order schemes can be detected shifts to larger

scales, here the scale is roughly $\sigma_2 \approx 1.5$ (Fig. 3e). Furthermore, the improvement is now very small. The power spectrum of higher order schemes is now than worse than first–order on small scales (Fig. 4e).

At stage 6 ($\sigma_2 = 2.0$) such a scale no longer exists, and we cannot appreciate any improvement of the higher-order schemes upon first-order. The break-down of the perturbation sequence is reached. To summarize, stage 3 ($\sigma_2 = 1.0$) is the last stage at which the improvement of second– and third–order schemes over first is large and positive. Increasingly in stage 4 and later differences become insignificant. There is substantial benefit at early stages from second–order, but there is never any important additional improvement by going to the third–order.

6. Conclusions

We have analyzed a time sequence of stages in a pancake model simulated numerically and compared with analytical Lagrangian perturbation solutions at various orders. We found that until the stage when σ_2(linear theory)$= 1$ (corresponding to the present epoch according to the standard normalization of large-scale structure models), the higher-order Lagrangian solutions clearly improve upon the first-order "Zel'dovich approximation" down to the resolution scale of the simulation. At later stages any small improvement can only be appreciated above a scale which increases with time until the stage σ_2(linear theory)≈ 1.5. Later stages correspond to the onset of hierarchical clustering, which are beyond the reach of the perturbation solutions at any order in this model. Also, third–order is computationally different and does not improve things much beyond second–order at any stage.

A typical feature of this break-down is the behavior of the higher-order schemes, which both become worse than the first-order scheme at later stages. This is due to the fact that in a perturbation approach the higher-order time coefficients grow more rapidly than the first-order time coefficient (here: $q_1 \propto a$, $q_2 \propto a^2$, $q_3 \propto a^3$). Consequently, the higher-order corrections blow up at and after the time coefficient functions are of the same order in all schemes which is the case roughly at the stage σ_2(linear theory)$= 1.5$. The limit (or break-down) scale k_b above which an improvement of the higher-order schemes upon the "Zel'dovich approximation" can be detected at about $\sigma_2(k_b) \approx 2$ corresponds to $R_G \approx 5$ and shifts to larger scales at later stages. After this stage we probe the onset of hierarchical clustering, for which the perturbation solutions are not meant for in the first place. Whether a truncation of the power spectrum in hierarchical models can retain the improvements detected here, will be analyzed in paper II. We also think that the break-down of the approximations must not be attributed to the lack of higher-order corrections. It might well be that the neglection of the self-gravitating interaction of streams in multi-stream regions by simply extrapolating the trajectories across caustics must be considered a major source of this break-down phenomenon.

We emphasize that both the N-body simulation and the Lagrangian perturbation solutions are assumed to be approximations to the unknown exact solution.

Another result of this paper is the relative importance of terms in the higher-order schemes, if we are concerned with the large-scale performance of the solutions in pancake models: We found that the vector perturbation potential $\mathcal{S}^{(3c)}$ can be safely neglected in this case. It will only be relevant if we resolve internal structures of pancakes. The same can be said for the third-order correction as a whole which does not improve upon the second-order scheme on large scales except with respect to the density distribution function at early stages. However, internal structures of pancakes are affected due to the

prediction of a third shell-crossing inside pancakes; also the collapse occurs substantially earlier than in the second-order model if calculated at high resolution (see Buchert *et al.* 1993). The higher core density in clusters as a result of this does not yield a noticeable improvement in the cross-correlation with the N-body simulation in the present case except a slight improvement of the cross-correlation of the third-order model on small scales at later stages. We also found that the realization of the third-order model is extremely sensitive to numerical errors by iteratively solving Poisson equations. A direct analytical calculation by explicitly solving the Poisson equations for a given model is more reliable but extremely CPU time extensive for a generic fluctuation field (see: Buchert *et al.* 1993). The second-order scheme which is much easier and faster to realize provides the main effect of improvement upon the "Zel'dovich approximation". It also provides a good compromise between improvement at early stages, while the surprisingly good performance of the first-order scheme on small scales at later stages is essentially preserved. Here we emphasize that the first impression of moderate improvement of second upon first order is misleading, since we compare with an approximation which already shows excellent agreement with the N-body result: e.g., the cross-correlation coefficient is already high in the first-order scheme. The latest stages analyzed here are in a regime where we are moving into hierarchical clustering. A removal of unwanted non-linearities by using, e.g., a Gaussian smoothing of the initial data will definitively change this picture (MPS). We will examine this when we study hierarchical models in paper II. We finally note that second-order solutions are available for a larger class of initial data than considered in this paper (Buchert & Ehlers 1993).

To summarize, without reservation we recommend the use of second–order perturbation theory up to the stage σ(linear theory)$= 1$, as a definite and useful improvement upon first–order (the "Zeldovich approximation") in pancake models.

The numerical code to realize Lagrangian perturbation solutions is available via e-mail: TOB @ ibma.ipp-garching.mpg.de .

Acknowledgements: We would like to thank Robert Klaffl for help during the preparation stage of this work and for valuable discussions as well as Jürgen Ehlers for valuable remarks on the manuscript.
TB is supported by DFG (Deutsche Forschungsgemeinschaft). ALM wishes to acknowledge support from NASA Grant NAGW–2923, NSF grants AST–9021414 and OSR–9255223, and facilities of the National Center for Supercomputing Applications, all in the USA.

References

Beacom J.F., Dominik K.G., Melott A.L., Perkins S.P., Shandarin S.F. (1991): *Ap.J.* **372**, 351.

Bertschinger E., Jain B. (1993): *Ap.J.*, in press.

Blanchard A., Buchert T., Klaffl R. (1993): *Astron. Astrophys.* **267**, 1.

Bouchet F.R., Juszkiewicz R., Colombi S., Pellat R. (1992): *Ap.J. Lett.* **394**, L5.

Buchert T. (1989): *Astron. Astrophys.* **223**, 9.

Buchert T., Bartelmann M. (1991): *Astron. Astrophys.* **251**, 389.

Buchert T. (1992): *M.N.R.A.S.* **254**, 729.

Buchert T. (1993a): *Astron. Astrophys. Lett.* **267**, L51.

Buchert T. (1993b): *M.N.R.A.S.*, in press.

Buchert T., Ehlers J. (1993): *M.N.R.A.S.* **264**, 375.

Buchert T., Karakatsanis G., Klaffl R., Schiller P. (1993): *Astron. Astrophys.*, to be submitted.

Chernin A.D. (1993): *Astron. Astrophys.* **267**, 315.

Coles P., Melott A.L., Shandarin S.F. (1993): *M.N.R.A.S.* **260**, 765.

Croudace K.M., Parry J., Salopek D.S., Stewart J.M. (1993): *Ap.J.*, in press.

Ehlers J., Buchert T. (1993): in preparation.

Giavalisco M., Mancinelli B., Mancinelli P.J., Yahil A. (1993): *Ap.J.* **411**, 9.

Gramann M. (1993): *Ap.J. Lett.* **405**, 47.

Kofman L.A., Pogosyan D., Shandarin S.F., Melott A.L. (1992): *Ap.J.* **393**, 437.

Lachièze-Rey M. (1993): *Ap.J.* **408**, 403.

Matarrese S., Lucchin F., Moscardini L., Saez V. (1992): *M.N.R.A.S.* **259**, 437.

Melott A.L. (1984): *Sov. Astron.* **28**, 631.

Melott A.L. (1986): *Phys. Rev. Lett.* **56**, 1992.

Melott A.L. (1987): *M.N.R.A.S.* **228**, 1001.

Melott A.L., Shandarin S.F. (1990): *Nature* **346**, 633.

Melott A.L., Pellman T.F., Shandarin S.F. (1993): *M.N.R.A.S.*, submitted.

Melott A.L., Shandarin S.F. (1993): *Ap.J.* **410**, 469.

Melott A.L. (1993): *Ap.J. Lett.* **414**, L73.

Moutarde F., Alimi J.-M., Bouchet F.R., Pellat R., Ramani A. (1991): *Ap.J.* **382**, 377.

Peebles P.J.E. (1980): *The Large-scale Structure of the Universe*, Princeton Univ. Press.

Peebles P.J.E. (1987): *Ap.J.* **317**, 576.

Shandarin S.F., Zel'dovich Ya.B. (1984): *Phys. Rev. Lett.* **52**, 1488.

Shandarin S.F., Zel'dovich Ya.B. (1989): *Rev. Mod. Phys.* **61**, 185.

Weinberg D.H., *et al.* (1993): in preparation.

Zel'dovich Ya.B. (1970): *Astron. Astrophys.* **5**, 84.

Zel'dovich Ya.B. (1973): *Astrophysics* **6**, 164.

Figure Captions

Figure 1: A thin slice (thickness $L/128$) of the density field is shown for the numerical (upper left), the first-order (upper-right), the second-order (lower left), and the third-order (lower right) approximations for the evolution stages 2 ($\sigma_2 = 0.5$, Fig. 1a), 3 ($\sigma_2 = 1.0$, Fig. 1b), 4 ($\sigma_2 = 1.2$, Fig. 1c), and 5 ($\sigma_2 = 1.5$, Fig. 1d). The grey-scale is linear, and the maximum density contrasts are chosen to be 8 in Fig. 1a, and 25 in Figs. 1b,c,d. (The slight stripes in low-density regions are artifacts resulting from the interaction of the distorted grid of the particles with the pixelization.)

Figure 2: The standard deviations of the density contrast as a function of smoothing scale R_G in the first-order (dotted), the second-order (dashed), the third-order (dashed-dotted), and the numerical (full line) approximations, for the evolution stages 1,2,3,4,5,6 (Figs. 2a,b,c,d,e,f). R_G is given in grid units; the shortest wave in the initial data was 32 grid units.

Figure 3: The cross-correlation coefficient S as a function of the standard deviation σ_2 for the evolution stages 1,2,3,4,5,6 (Figs. 3a,b,c,d,e,f). The cross–correlation of the N-body with first-order perturbation theory is shown as a dotted line; with second-order a dashed line; and with third-order a dashed-dotted line.

Figure 4: The power spectra of the N-body simulation (solid line) compared with the first- (dotted), second- (dashed), and third-order (dashed-dotted) approximation schemes for the stages $1, 2, 3, 4, 5, 6$ (Figs. 4a,b,c,d,e,f).

Figure 5: The relative phase-errors. Notation and labelling like in Figure 3.

Figure 6: The density distribution functions. Notation and labelling like in Figure 4.

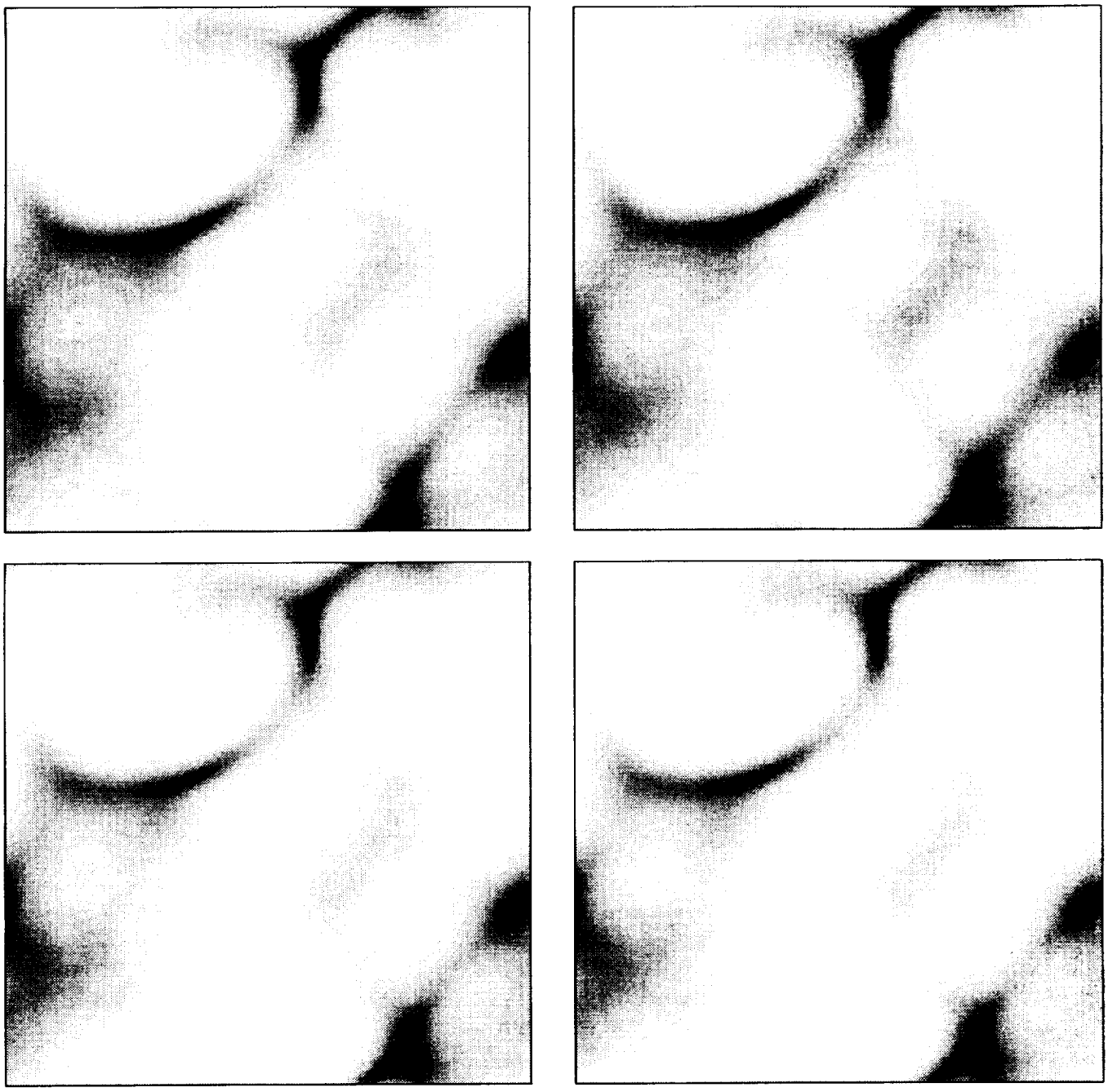

Figure 1a

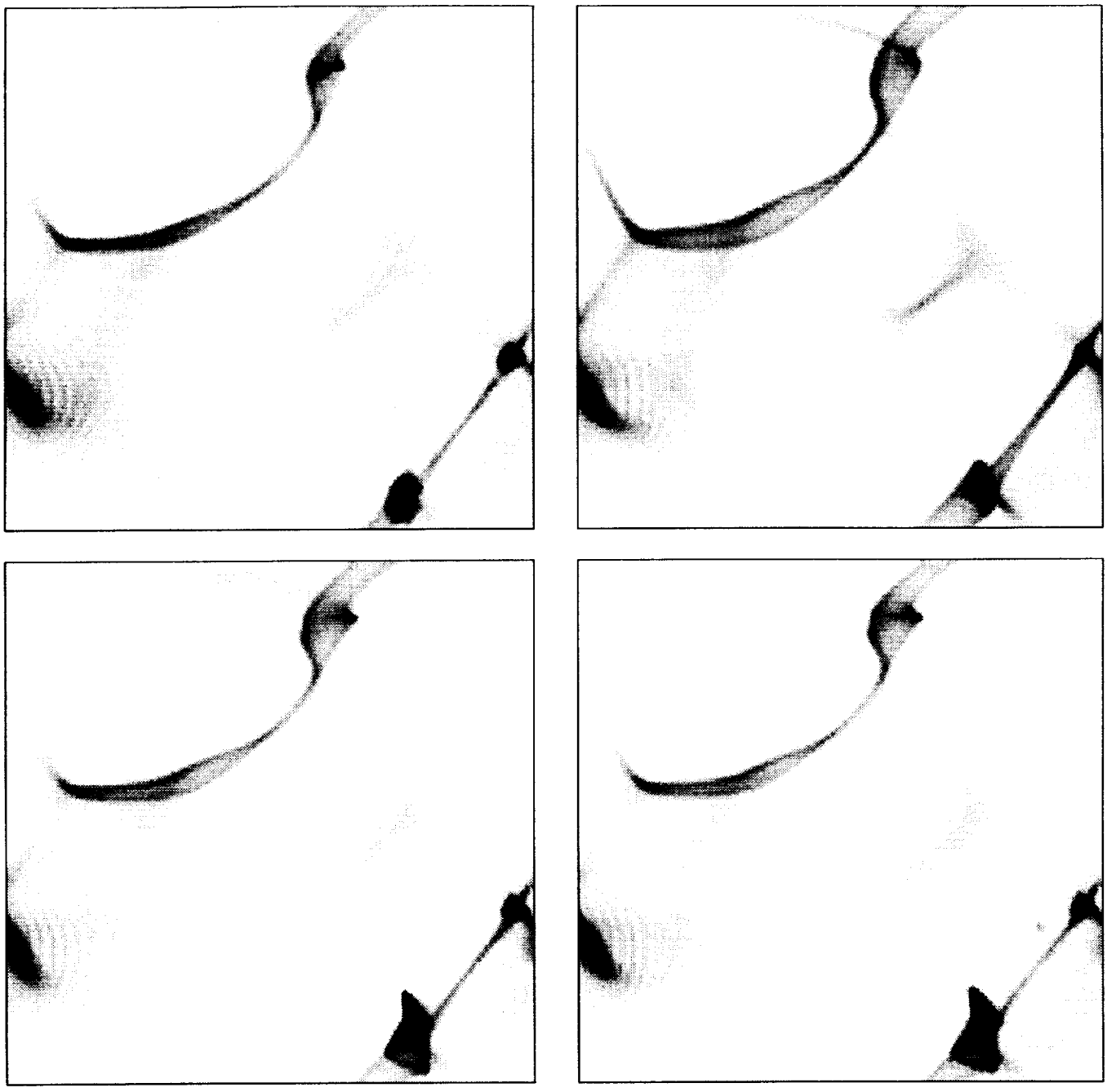

Figure 1b

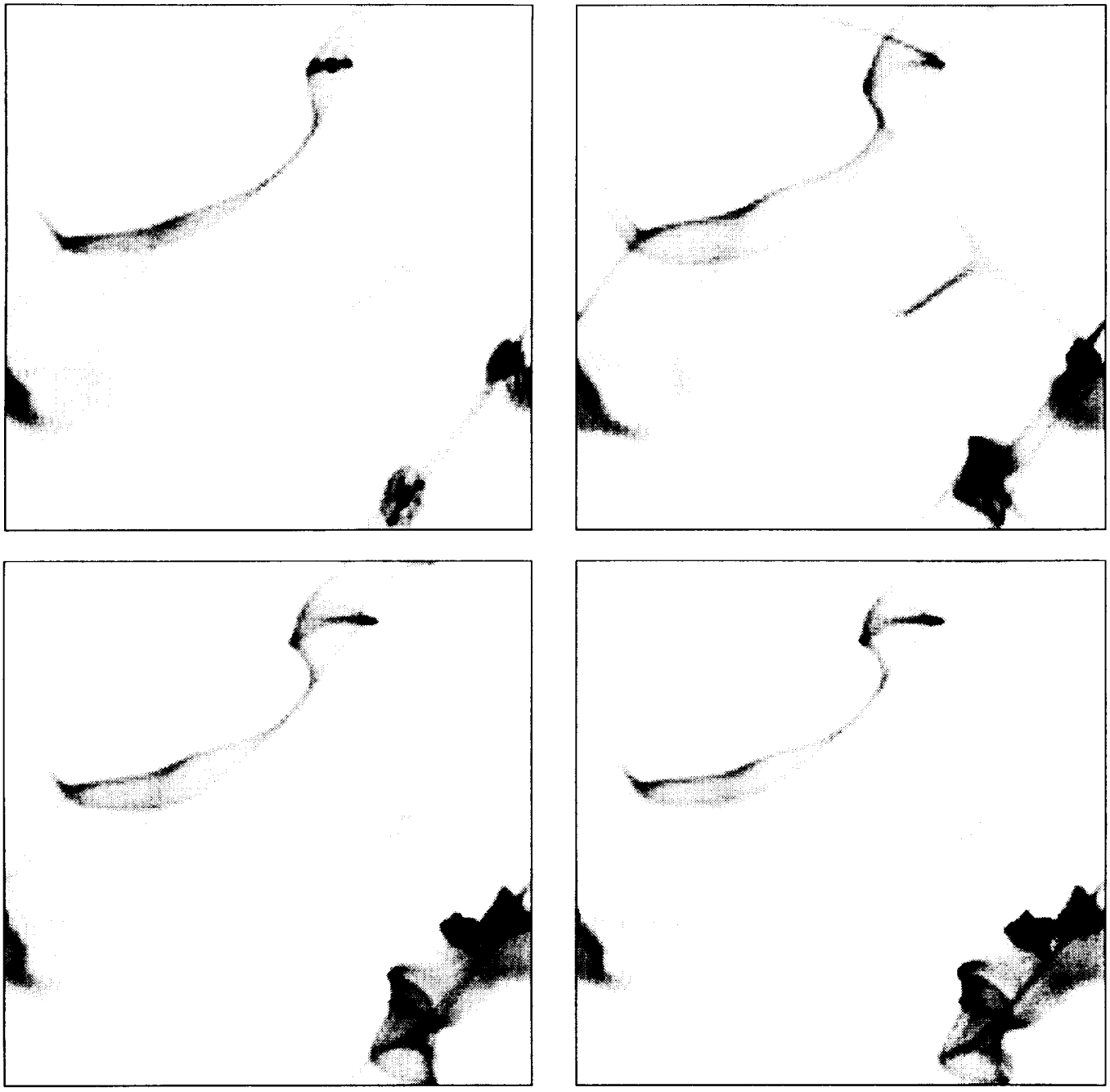

Figure 1c

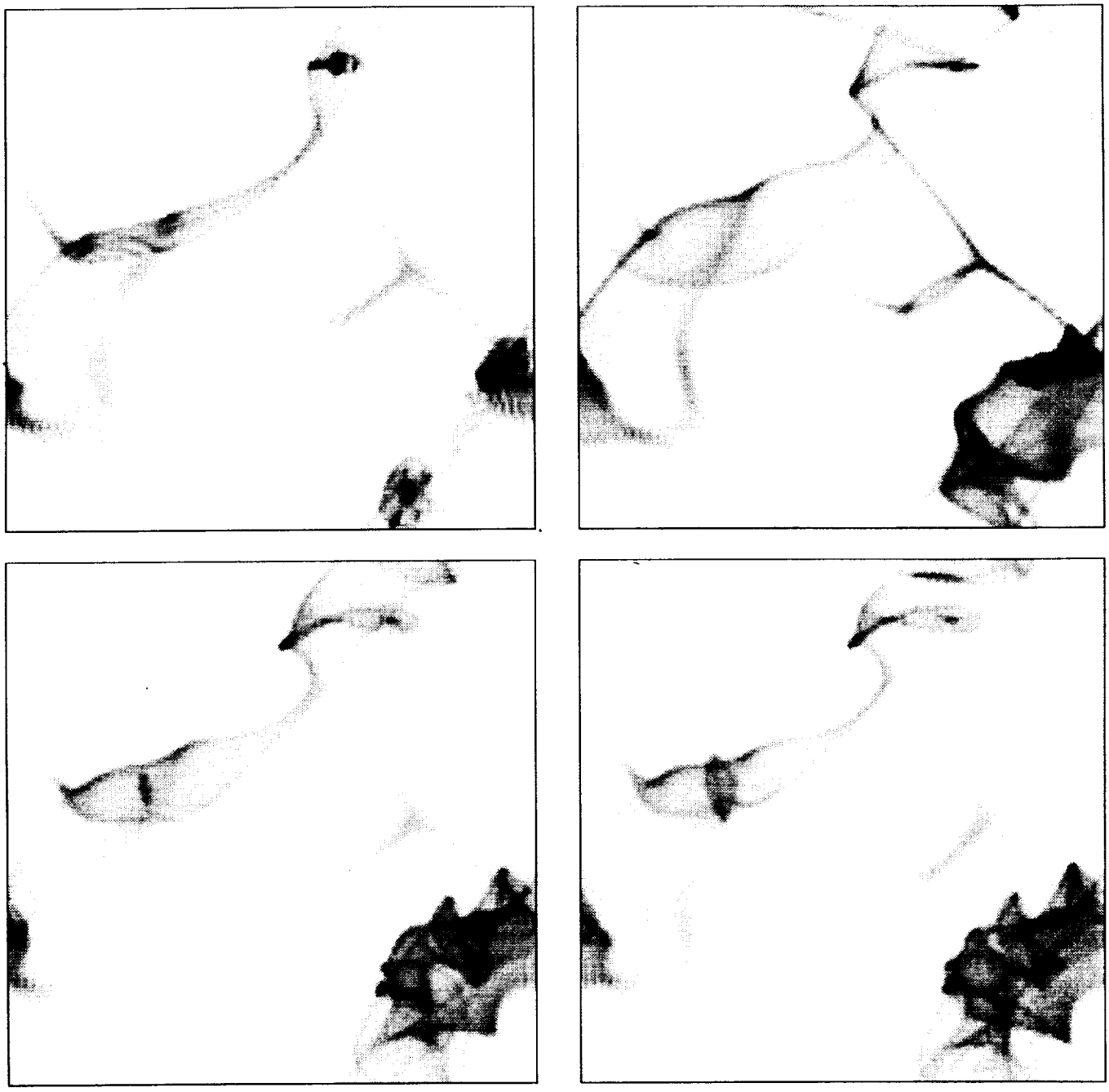

Figure 1d

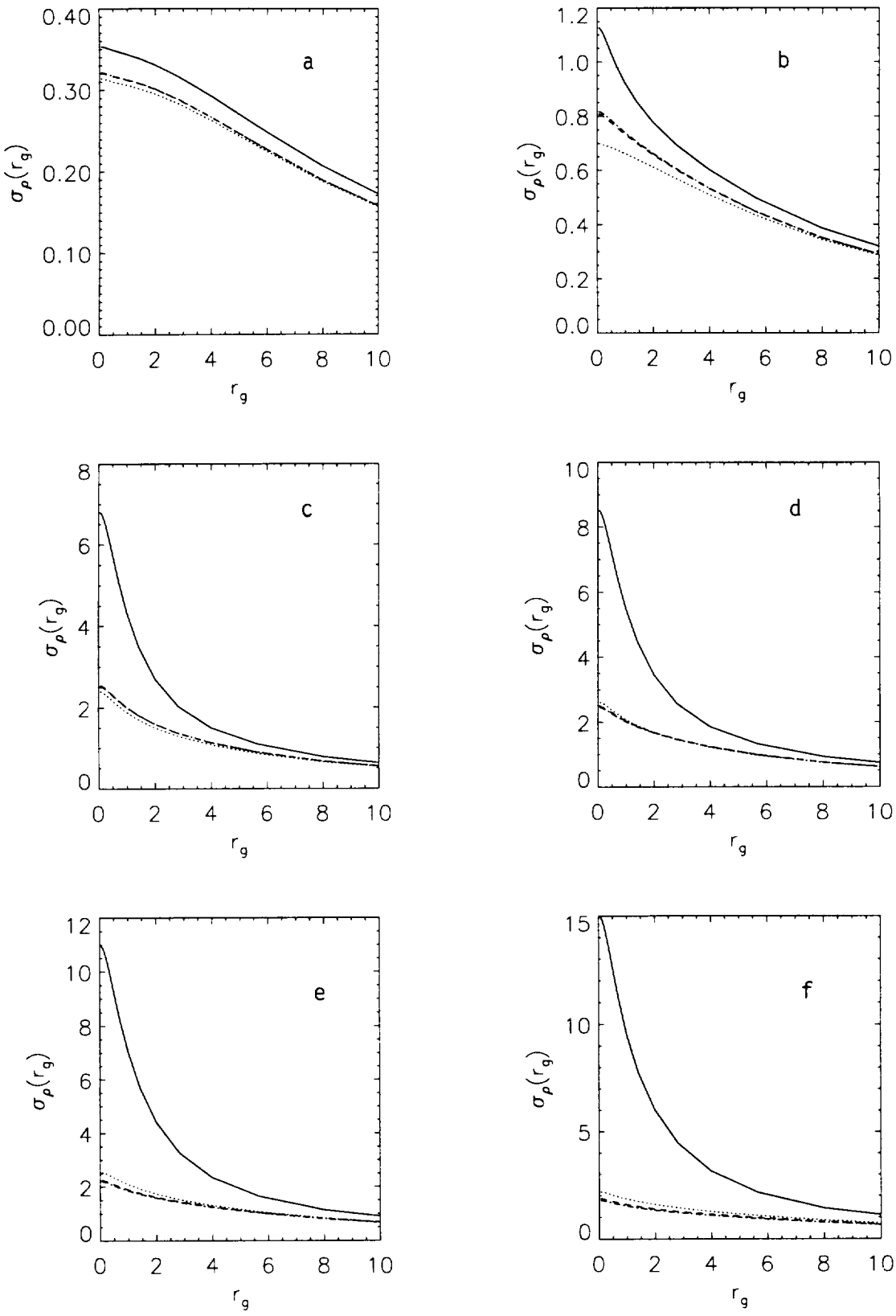

Figure 2

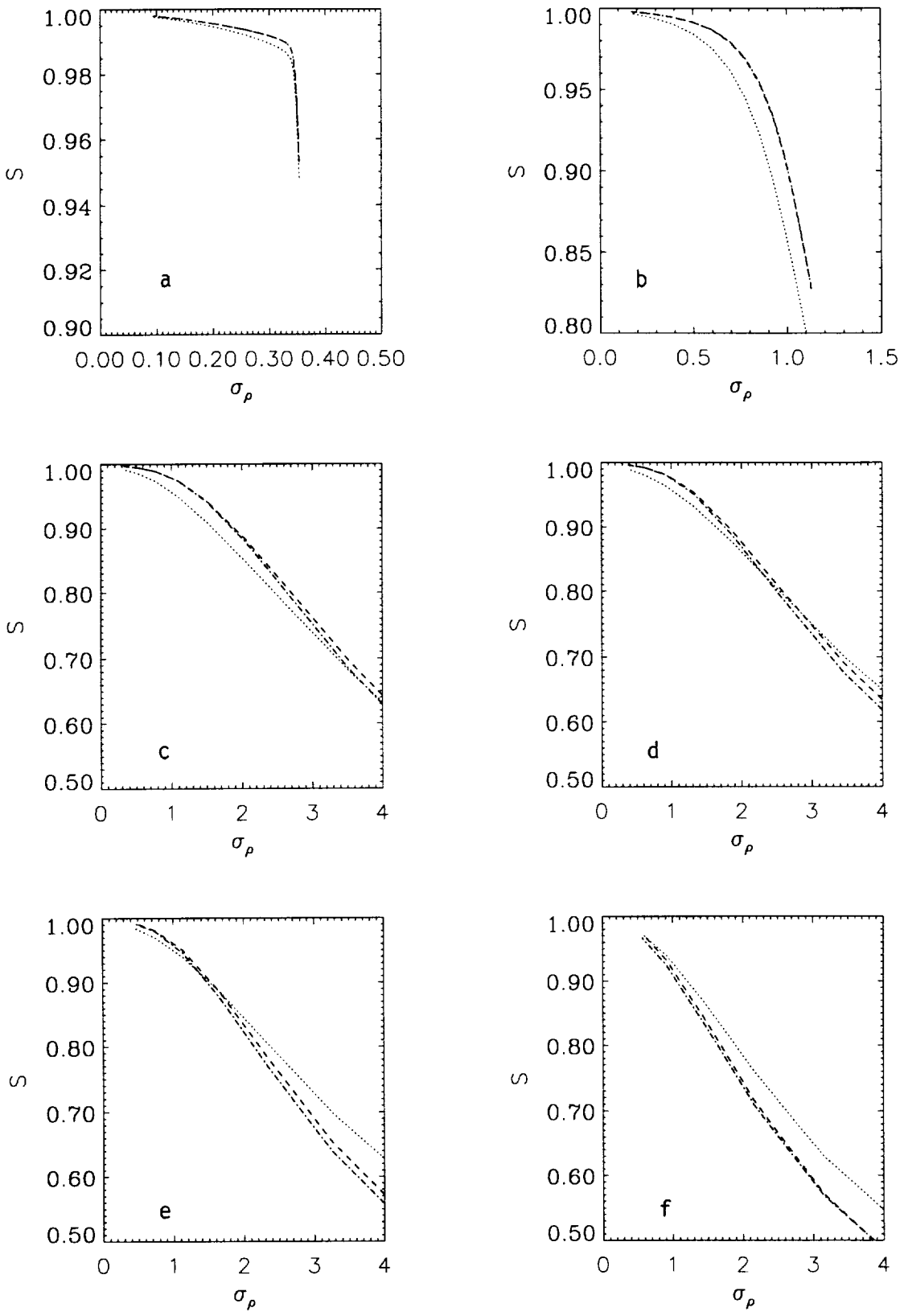
1.00
0.98
0.96
0.94
0.92
0.90
S
a
0.00 0.10 0.20 0.30 0.40 0.50
σ_ρ
1.00
0.95
0.90
0.85
0.80
S
b
0.0 0.5 1.0 1.5
σ_ρ
1.00
0.90
0.80
0.70
0.60
0.50
S
c
0 1 2 3 4
σ_ρ
1.00
0.90
0.80
0.70
0.60
0.50
S
d
0 1 2 3 4
σ_ρ
1.00
0.90
0.80
0.70
0.60
0.50
S
e
0 1 2 3 4
σ_ρ
1.00
0.90
0.80
0.70
0.60
0.50
S
f
0 1 2 3 4
σ_ρ

Figure 3

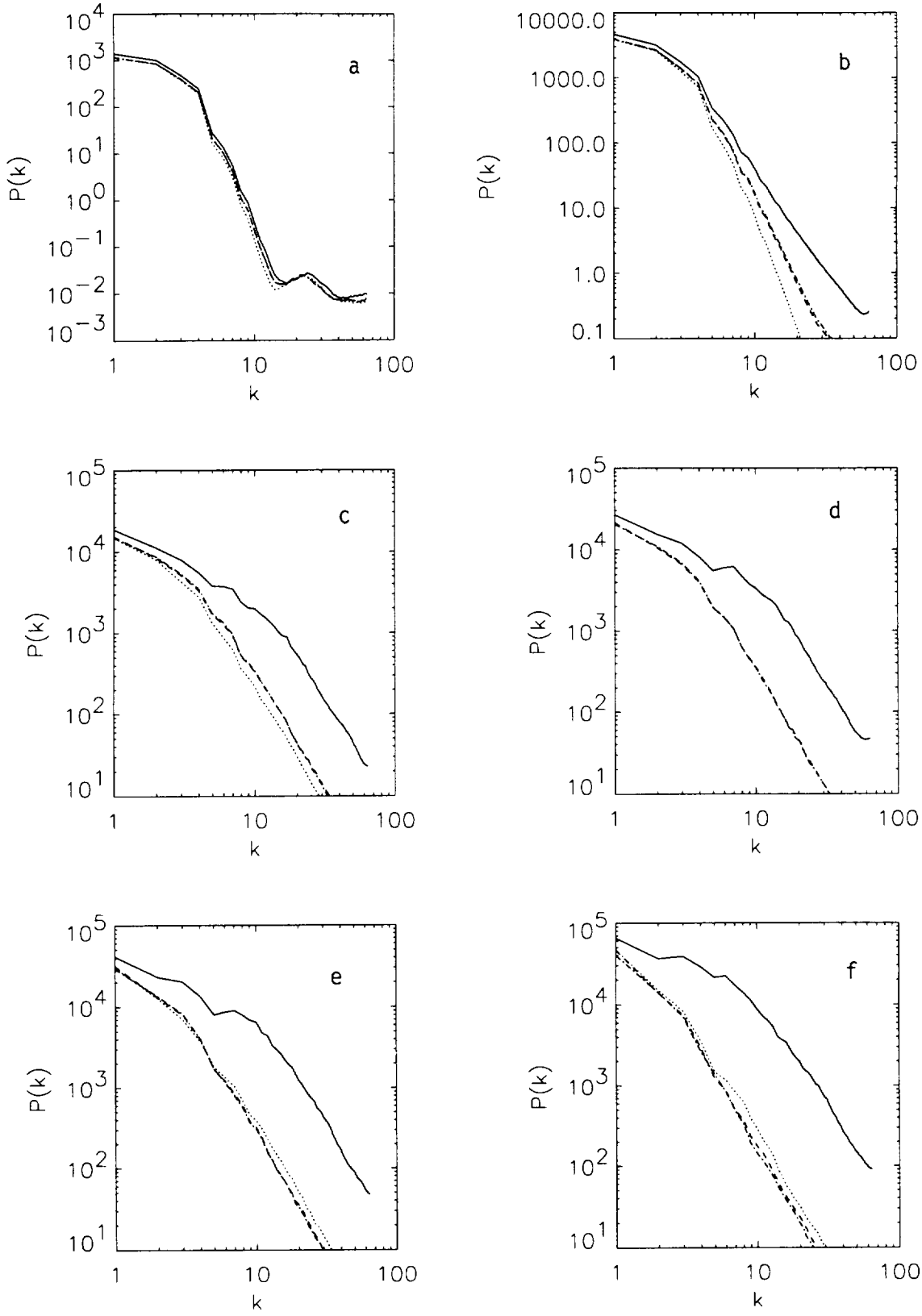
a
b
c
d
e
f
P(k)
k
1
10
100
10^{-3}
10^{-2}
10^{-1}
10^{0}
10^{1}
10^{2}
10^{3}
10^{4}
10^{5}
0.1
1.0
10.0
100.0
1000.0
10000.0

Figure 4

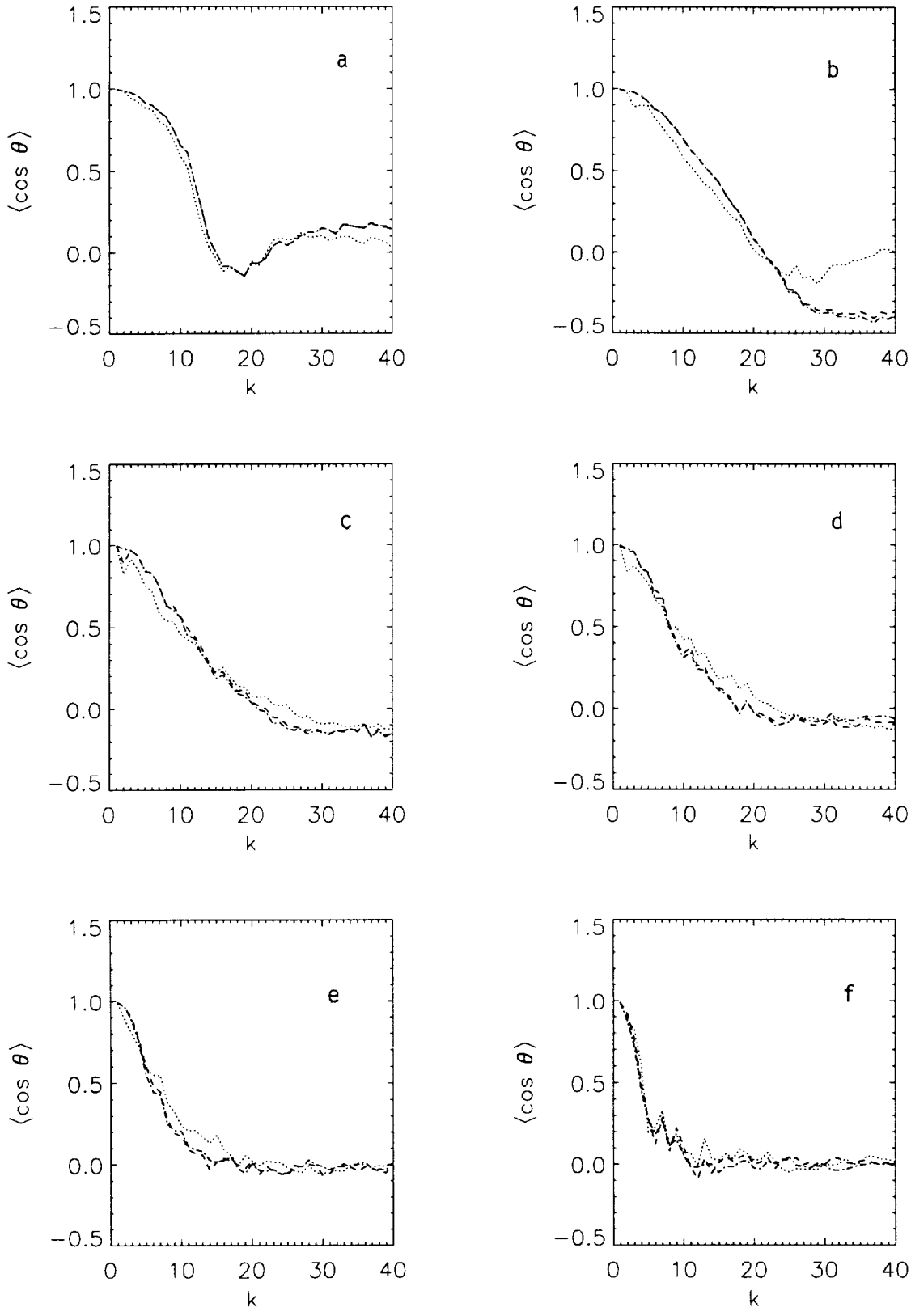

Figure 5

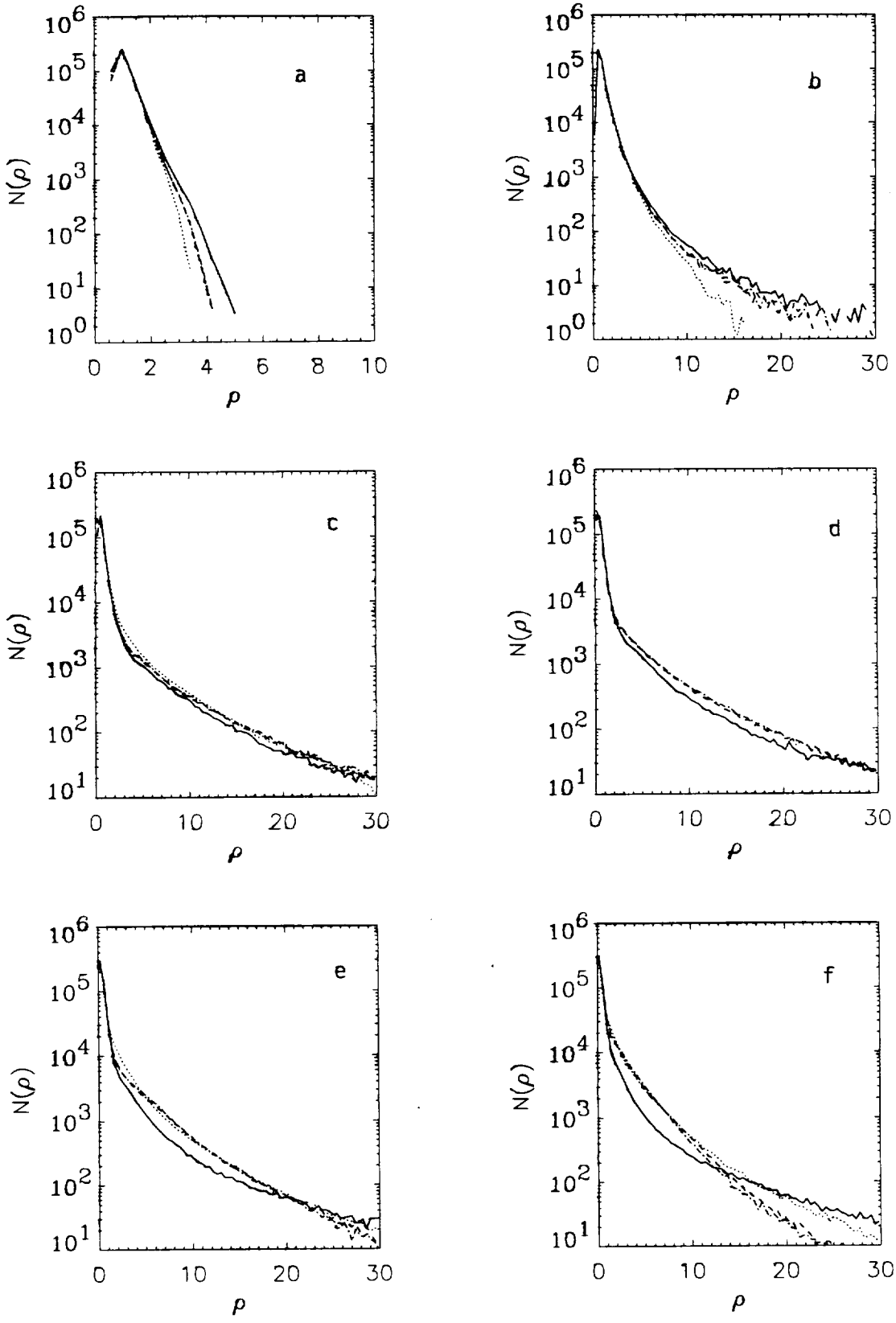

Figure 6